Article

Iron Chelation Nanoparticles with Delayed Saturation as an Effective Therapy for Parkinson Disease

Nan Wang, Xin Jin, Dongbo Guo, Gangsheng Tong, and Xinyuan Zhu

Biomacromolecules, **Just Accepted Manuscript** • DOI: 10.1021/acs.biomac.6b01547 • Publication Date (Web): 19 Dec 2016

Iron Chelation Nanoparticles with Delayed Saturation as an Effective Therapy for Parkinson Disease

Nan Wang,[1] Xin Jin,[1,*] Dongbo Guo,[1] Gangsheng Tong,[2] Xinyuan Zhu[1,*]

[1]*School of Chemistry and Chemical Engineering, State Key Laboratory of Metal Matrix Composites, Shanghai Jiao Tong University, 800 Dongchuan Road, Shanghai 200240, P. R. China*

[2]*Instrumental Analysis Center, Shanghai Jiao Tong University, 800 Dongchuan Road, Shanghai 200240, P. R. China*

* Corresponding authors. E-mail: X. Z. (xyzhu@sjtu.edu.cn); X. J. (jxcindy@sjtu.edu.cn). Telephone: +86-21-54746215. Fax: +86-21-54741297.

ABSTRACT: Iron accumulation in substantia nigra pars compacta (SNpc) has been proved to be a prominent pathophysiological feature of Parkinson's diseases (PD), which can induce the death of dopaminergic (DA) neurons, up-regulation of reactive oxygen species (ROS), and further loss of motor control. In recent years, iron chelation therapy has been demonstrated to be an effective treatment for PD, which has shown significant improvements in clinical trials. However, the current iron chelators are suboptimal due to their short circulation time, side effects and lack of proper protection from chelation with ions in blood circulation. In this work, we designed and constructed iron chelation therapeutic nanoparticles protected by a zwitterionic poly(2-methacryloyloxyethyl

phosphorylcholine) (PMPC) to delay the saturation of iron chelators in blood circulation and prolong the *in vivo* life time, with HIV-1 trans-activating transcriptor (TAT) served as a shuttle to enhance the blood-brain barrier (BBB) permeability. We explored and investigated whether the Parkinsonian neurodegeneration and the corresponding symptoms in behaviors and physiologies could be prevented or reversed both *in vitro* and *in vivo*. The results demonstrated that iron chelator loaded therapeutic nanoparticles could reverse functional deficits in Parkinsonian mice not only physiologically but also behaviorally. On the contrary, both untreated PD mice and non-TAT anchored nanoparticle treated PD mice showed similar loss in DA neurons and difficulties in behaviors. Therefore, with protection of zwitterionic polymer and prolonged *in vivo* life time, iron chelator loaded nanoparticles with delayed saturation provide a PD phenotype reversion therapy and significantly improve the living quality of the Parkinsonian mice.

KEYWORDS: zwitterionic polymer; iron chelator; Parkinson's disease; delayed saturation; long circulation

INTRODUCTION

Injuries to the central nervous system (CNS) can give rise to destructive consequences.[1,2] Parkinson's disease (PD) is considered as the second most common progressive neurodegenerative movement disorder of CNS associated with a selective loss of dopaminergic neurons in substantia nigra pars compacta (SNpc), especially among aged people.[3-6] The progress of PD is characterized by motor impairment, autonomic dysfunction, many psychological and cognitive changes.[7-11] The pathogenetic mechanisms associated

with neuronal degeneration in PD are complicated and remain to be fully clarified. In past few decades, increasing evidence has suggested that oxidative stress is the key factor for the loss of dopaminergic neurons in PD,[9-14] while Fenton reaction caused by the abnormal accumulation of iron can generate excess reactive oxygen species (ROS) and further aggravate oxidative stess.[15-17] The abnormal iron accumulation in PD eventually leads to the death of dopaminergic neurons and loss of motor control.[18-25] Therefore, iron chelation therapy has proved to be an effective modality for PD in several ways.[26-31]

Nowadays, extensive attention has been focused on the design and fabrication of novel iron chelators. Desferrioxamine (DFO),[32-35] clioquinol (CQ),[36,37] extracts from green and black tea[38,39] and selective propargyl containing monoamine oxidase (MAO) AB inhibitors, such as 5-(4-(2-hydroxyethyl) piperazin-1-ylmethyl)-8-hydroxyquinoline (VK-28), 5-(*N*-methyl-*N*-propargyaminomethyl)-8-hydroxyquinoline (M30) and 5-(*N*-propargylaminomethyl)-8-hydroxyquinoline (M30A),[40-45] have shown powerful iron chelating ability, antioxidation and neuroprotection in the treatment of PD even in clinical trials. However, the therapeutic effect of current iron chelators is usually impeded due to their short *in vivo* circulation time, cytotoxicity to some extent and saturation before reaching the lesion sites in brain.[29]

However, it's surprising to find that few attention has been paid in the available iron chelation ability at the sites of neuronal lesions after entering brain, which should be a key factor for the final therapeutic efficacy of PD. Lack of proper protection from various free ions in blood circulation, iron chelators will be saturated before reaching lesion sites, and lose their capacity to chelate with irons inside brain. Nowadays, satisfactory iron chelating

therapies are still urgently in need to moderate or suppress the disease progression of PD.[46,47] An ideal iron chelator should possess particular features such as high iron binding affinity, brain-permeability, non-toxicity, long *in vivo* life time and the most important character of delayed saturation in blood circulation, which can shield properly from unnecessary chelation with free ions in plasma circulation. Jiang and co-workers have demonstrated that zwitterionic polymer polycarboxybetaine (PCB) can prevent the nonspecific interactions between encapsulated stem cells and external biochemical substances due to the hydration layer on the surface.[48-50] As a family member of zwitterionic polymers, poly(2-methacryloyloxyethyl phosphorylcholine) (PMPC) shows similar hydrophilicity, biocompatibility, stability and non-fouling property with PCB.[51-55] Therefore, we hypothesize that PMPC encapsulation can provide a suitable protection for the loaded iron chelator from surrounding chemical ions during blood circulation. Moreover, PMPC will endow the delivery system much longer circulation-life time *in vivo* with better chance to contact with and penetrate through the blood-brain barrier (BBB).

To verify the importance of proper protective layer out of the iron chelators, we report here for the first time a novel PD therapeutic iron chelator system with zwitterionic polymer PMPC as a hydration protective layer on the surface, which possesses delayed saturation feature to prevent iron-induced Fenton reaction and the generation of ROS in brain. In this work, we choose non-Fe hemin (NFH) as a natural prototype iron chelator, which is obtained *via* removing iron core of hemin as previously described.[56] Moreover, one molecule of hemin contains one molecule of iron, which means that the binding affinity between chelator and iron ion in molar ratio is 1 to 1, higher than most current therapeutic iron chelators.[57-59]

Thus by using NFH as iron chelator, we can lower the dose of iron chelator to achieve the same level of therapeutic efficacy. Due to its excellent ability to deliver a variety of cargos through the BBB, HIV-1 trans-activating transcriptor (TAT) is covalently conjugated onto the iron chelator system and served as a shuttle to enhance the BBB permeability of therapeutic nanoparticles.[60-62]

EXPERIMENTAL SECTION

Materials. Bovine serum albumin (BSA), 1-(3-dimethylaminopropyl)-3-ethylcarbodiimide hydrochloride (EDC), dimethyl sulfoxide (DMSO), hemin-Cl, chloroform ($CHCl_3$), hydrochloric acid (HCl), trimethylamine and sodium hydrogen carbonate ($NaHCO_3$) were purchased from Aladdin Reagent Database Inc. (Shanghai, China). Acrylic acid (AA), *N*-hydroxy-succinimide ester (NAS), *N*,*N*′-methylene bisacrylamide (BIS), ammonium persulfate (APS), 2-methacryloyloxyethyl phosphorylcholine (MPC), *N*,*N*,*N*′,*N*′-tetramethylethylenediamine (TEMED), *N*-hydroxysuccinimide (NHS) and 1-methyl-4-phenyl-1,2,3,6-tetrahydropyridine (MPTP) were all purchased from Sigma-Aldrich Co. LLC. (USA). TAT (GRKKRRQRRRPP-CH_3O) was purchased and synthesized by Shanghai Science Peptide Biological Technology CO., LTD. (Shanghai, China).

Characterization. *Dynamic Light Scattering (DLS).* DLS was used to measure the size, size distribution and zeta potential of particles in aqueous solution carried out with a Malvern Zetasizer Nano S instrument (Malvern Instruments Ltd) equipped with a 4.0 mW He-Ne

laser operating at λ = 633 nm. All samples (0.5 mg mL^{-1} of BSA) were measured at a scattering angle of 90 °in 20 mM phosphate buffer (PB) at room temperature (25 ℃).

Transmission Electron Microscopy (TEM). TEM studies were performed with a Tecnai G2spirit Biotwin instrument at a voltage of 120 kV (FEI, USA). Samples were prepared by dropping the solutions onto carbon-coated copper grids followed by air-drying at ambient temperature. Then the samples were negative stained by 1% phosphotungstic acid (pH 7.0) before measurement.

^{31}P Nuclear Magnetic Resonance Spectroscopy (NMR). ^{31}P NMR spectra were recorded using a Varian Mercury Plus 400 MHz spectrometer to confirm the attachment of PMPC onto the nanoparticles. Samples were prepared by dissolving in 50% H_2O/50% D_2O at 0.25 mg mL^{-1} and pH was adjusted to 7.4.

Flow Cytometry (FCM). FCM was assessed using flow cytometer (Accuri C6, Becton, Dickinson and Company, Shanghai, China). TAT was labeled with FITC in pH 8.5, 20 mM PB. Non-TAT modified (used as control to draw the gate) and FITC-labeled TAT-modified nanoparticles were recorded in flow cytometer to affirm the attachment of TAT onto the system.

Ultraviolet-Visible Spectrophotometer (UV-vis). UV-vis absorption of the sample solutions was measured with a Thermo Electron-EV300 UV-vis spectrophotometer at room temperature. The slit-width was set as 1 nm with a scan speed of 480 nm min^{-1} from 200 nm to 700 nm.

Inductively Coupled Plasma - Atomic Emission Spectrometry (ICP-AES). ICP-AES was used to analyze the samples of both purchased hemin-Cl and non-Fe hemin-Cl (NFH) on a Thermo, USA, iCAP6300 instrument. All samples were spiked with 1% nitric acid to aid analysis.

Sodium Dodecyl Sulfate - Polyacrylamide Gel Electrophoresis (SDS-PAGE). SDS-PAGE was carried out to determine the molecular weight of the nanoparticles. Native BSA, nBSA, TAT-modified three systems were used as samples and Protein Ladder (purchased from Beyotime, Shanghai, China) was used as the marker. Precast gel was purchased from Willget Biotech Co., Ltd, Shanghai, China. After stained and decolourization for three days, the result was shown in BIO-RAD Gel Doc XR+ (BIO-RAD, USA).

Preparation of Acrylated BSA Protein (aBSA). BSA protein was dissolved in 20 mM pH 8.5 boric acid buffer (BB) solution to prepare a BSA solution with a concentration of 1.0 mg mL^{-1}. 31.0 μL 1% (w/w) DMSO solution of NAS was introduced to 13.3 mL BSA solution. The mixture was stirred for 2 h at room temperature, and then dialyzed (MWCO: 7000 Da) against 20 mM phosphate buffer (PB, pH 7.4) solution for 48 h (fresh PB solution was replaced every 6 h) to give an aBSA solution.

Preparation of Non-Fe Hemin-Cl (NFH). The wipe out of irons from the purchased hemin-Cl was carried out as previously described by Jayawickramarajah's group.[56] 10 drops of concentrated HCl were added to a solution of hemin-Cl (40.0 mg, 61.0 mmol) in 100.0 mL $CHCl_3$, and then continued to stir for another 10 min. The reaction mixture was successively neutralized to pH 7.0 with trimethylamine and washed with 200.0 mL saturated

$NaHCO_3$ solution. Then, the product of NFH was obtained as a black solid over rotary evaporator. NFH was kept in DMSO as 10.0 mg mL^{-1}.

Preparation of Zwitterionic Polymer Capsuled Protein-Based Nanoparticle (nBSA). The typical procedure for the preparation of zwitterionic polymer capsuled protein-based nanogel *via* radical polymerization from the surface of acryloylated protein is described as below: an aqueous solution of 118.1 mg MPC, 15.0 mg BIS, 29.4 μL TEMED and the above 5.0 mL 0.5 mg mL^{-1} aBSA solution was added to a 25 mL flask. The mixture was bubbled with nitrogen for 0.5 h to remove residual oxygen at room temperature. Then 11.0 mg APS was rapidly added into the flask to initiate the polymerization. The reaction was allowed to proceed for an additional 3 h in a nitrogen atmosphere at room temperature. Finally, dialysis (MWCO: 100 kDa) was used to remove monomers and initiators in 20 mM PB solution (pH 7.4) for 48 h (fresh PB solution was replaced every 6 h) to give an nBSA solution.

Preparation of NFH Loaded Zwitterionic Nanoparticle (NFH-nBSA). The preparation of drug loaded nanoparticle was similar to that of nBSA nanoparticle by loading the drug onto the nanoparticle. NFH (10.0 mg mL^{-1}, 1.6 mL), EDC (4.5 mg) and NHS (2.5 mg) were added to the aBSA nanoparticle solution (0.5 mg mL^{-1}, 16.0 mL) and stirred for 3 h. The solution was dialyzed (MWCO: 100 kDa) against 20 mM PB (pH 7.4) for 48 h to give the drug loaded nanoparticle NFH-aBSA. Then an aqueous solution of 118.1 mg MPC, 15.0 mg BIS, 29.4 μL TEMED and the above 10.0 mL 0.5 mg mL^{-1} NFH-aBSA solution was added to a flask. The mixture was bubbled through nitrogen for 0.5 h to remove residual oxygen at room temperature. Then 11.0 mg APS was rapidly added and the polymerization was allowed to continue for another 3 h in a nitrogen atmosphere at room temperature. Finally,

dialysis (MWCO: 100 kDa) was used to remove monomers and initiators in 20 mM PB solution (pH 7.4) for 48 h to give NFH-nBSA nanoparticle.

Bioconjugation of TAT with Zwitterionic Nanoparticle (TAT-NFH-nBSA). The bioconjugation of cell penetrating peptide TAT with zwitterionic and protein-based nanoparticle were similar to that of BSA nanoparticle by modifying the protein-based nanoparticle using a conjugating technique. An aqueous solution of 118.1 mg MPC, 1.4 μL AA, 15.0 mg BIS, 29.4 μL TEMED and the above 10.0 mL 0.5 mg mL^{-1} NFH-aBSA solution was added to a flask. The mixture was bubbled through nitrogen for 0.5 h to remove residual oxygen at room temperature. Then 11.0 mg APS was rapidly added and the polymerization was allowed to proceed for an additional 3 h in a nitrogen atmosphere at room temperature. Finally, dialysis (MWCO: 100 kDa) was used to remove monomers and initiators in 20 mM PB solution (pH 7.4) for 48 h. After that, EDC (4.3 mg) and NHS (2.3 mg) were added to the BSA-based nanoparticle solution (0.5 mg mL^{-1}, 5.0 mL) and stirred for 3 h. At last, different amount of TAT (1.0 mg mL^{-1} in DMSO) was added to this mixture and stirred for another 3 h (60.4 μL TAT for TAT-1-NFH-nBSA, 302.0 μL TAT for TAT-5-NFH-nBSA and 604.0 μL TAT for TAT-10-NFH-nBSA, and the number stands for the molar ratio of TAT to BSA). The solution was dialyzed (MWCO: 100 kDa) against 20 mM PB (pH 7.4) for 48 h to give the final nanoparticle solution.

Cell Culture. SH-SY5Y (Human bone marrow neuroblastoma cell) was purchased from Shanghai Institute for Biological Sciences, Chinese Academy of Sciences Institute of Cell Resource Center (Shanghai, China). SH-SY5Y cells were cultured in the medium of

DMEM/ F12k (1:1) with 10% FBS and 1% penicillin-streptomycin. Cells were cultured in a humidified atmosphere at 37 ℃ with 5% CO_2.

Animals. BalB/C, KM and C57BL/6 mice were purchased from Shanghai SLAC Laboratory Animal CO. LTD. (Shanghai, China). The animals were housed with free access to food and water in the specific pathogen-free (SPF class) animal room. The protocol of animal experiments was approved by the Animal Experimentation Ethics Committee of Shanghai Jiao Tong University School of Pharmacy.

Detection of Free Fe Ions in C57BL/6 Mice Blood Serum. For determination of free Fe ions in mice blood serum, the blood was drawn from the retinal vein plexus of 10 healthy C57BL/6 mice (6 week, male), and collected in separation gel coagulation promoting tubes firstly to get rid of the blood cells from the blood as the protein contained serum. Then the prepared serum was centrifuged to remove all the macromolecular substances with only small molecules in (10,000 rpm, 10 min ×3) with ultrafiltration tubes (MWCO: 5 kDa). The concentration of free Fe ions in the serum was determined with ICP-AES on a Thermo, USA, iCAP6300 instrument.

Assessment of Fe(II)-Binding Capacity *In Vitro.* The iron chelating ability of different systems was determined by evaluating their ability to compete with ferrozine (3-[2-pyridyl]-5,6-diphenyl-1,2,4-triazine-4,4'-disulfonic acid) for chelating ferrous ions, leading to absorbance reduction of ferrozine-Fe(II) complex at 562 nm. The tests were preceeded in 5% ammonium acetate buffer (pH 6.9). Various concentrations of free NFH, NFH-nBSA, TAT-NFH-nBSA (10, 40, 100 μM of NFH, in duplicate) were incubated with $FeSO_4$ (2, 15 μM)

for 30 min (the sample without NFH treated was set as control), and then added 300 μM ferrozine (Sigma-Aldrich). After another 30 min of incubation at room temperature, the absorbance of the resulting solutions at 562 nm was get with Thermo Electron-EV300 UV-vis spectrophotometer. The Fe(II)-chelating effect and the saturability at the corresponding concentration were calculated as follows:

$$\text{Iron Chelating Effect (\%)} = [1-(\text{Abs}_{562\ \text{nm}}\ \text{of sample})/\ (\text{Abs}_{562\ \text{nm}}\ \text{of control})] \times 100$$

$$\text{Saturability (\%)} = (\text{Conc. of } Fe^{2+} \times \text{Iron Chelating Effect (\%)}/\text{Conc. of NFH}) \times 100$$

***In Vitro* Cytotoxicity of Materials.** The cytotoxicity of delivery system was assessed using MTT assay. SH-SY5Y cells were seeded in a 96-well plate at a cell density of 1.0×10^4 cells per well and incubated for 24 h at 37 ℃ and 5% CO_2 before they were treated with different concentration of free NFH, NFH-nBSA and TAT-NFH-nBSA, respectively. All samples were incubated with the cells for 24 h. Before MTT assay, each well was refilled with fresh medium. For MTT assay, 20.0 μL of 5.0 mg mL^{-1} MTT (Beyotime Institute of Biotechnology, Shanghai, China) solution was added to each well and incubated for 4 h at 37 ℃. After dissolving the formed formazan with 150.0 μL DMSO in each well, the plates were shaken for 5 min with the shaker. The absorbance was measured at 490 nm with microplate reader. The cytotoxicity was measured by comparing the absorbance of each concentration with control group.

***In Vitro* Anti-Parkinson Effects of Drug-Loaded Nanoparticle.** SH-SY5Y cells were chosen to evaluate the anti-Parkinson effects of NFH-loaded nanoparticle by MTT assay. The cells were seeded in 96-well plates at a density of 1.0×10^4 cells per well in 200 μL

medium. After 24 h incubation, the cells obtained 70-80% confluence. Then the culture medium was removed and replaced with 200 μL fresh medium. The cells were treated with 100 μL MPTP (300 μmol L^{-1}) per well for 1 h to give Parkinsonian (PD) cells. Then serial dilutions of free NFH, NFH-nBSA and TAT-NFH-nBSA nanoparticle were added into each well. The cells without treatment were set as control. The cells were cultured for another 48 h at 37 ℃ under 5% CO_2. Before MTT assay, each well was refilled with fresh medium. Thereafter, 20 μL of MTT solution (5 mg mL^{-1} in PBS) was added to each well and the cells were incubated for another 4 h. Then culture medium was removed and 200 μL DMSO was added into each well to dissolve the formazan crystals. Then the plates were vibrated for 10 min and the absorbance of each well was measured in a BioTek® Synergy H4 microplate reader at a wavelength of 490 nm. The anti-Parkinson effects were measured by comparing the absorbance of each concentration with control group.

***In Vitro* ROS Level Reverse Effects of Parkinsonian Cell.** The reverse effects of PD cells of the NFH-loaded nanoparticles were evaluated with analysis of intracellular ROS levels of the PD cells. Meanwhile, the untreated healthy cells and PD cells were used as controls. The levels of ROS in SH-SY5Y cells were examined and determined by flow cytometry (Accuri C6, BD). DCFH-DA is a cell-permeable non-fluorescent probe which can be de-esterified intracellularly and turns to highly fluorescent DCFH which is non-cell-permeable. SH-SY5Y cells were seeded in 24-well plates at a density of 5.0×10^4 cells per well in 1 mL medium. After 24 h incubation, the cells obtained 70-80% confluence. The culture medium was removed and replaced with 1 mL fresh medium. Then the cells were treated with 100 μL MPTP (300 μmol L^{-1}) per well for 1 h to give PD cells and generate

ROS. The healthy control was treated with 100 μL PB (20 mM). The PD cells were treated with 62.5 μL selected concentration of NFH-nBSA and TAT-NFH-nBSA, respectively. The healthy group (set as control group) and PD group were treated with 62.5 μL PB (20 mM). The cells were cultured for another 24 h at 37 ℃ under 5% CO_2. Cells were harvested and resuspended in 500 μL non-serum medium with 10 μM DCFH-DA solution, incubated at 37 ℃ for 30 min, washed with non-serum medium three times, analyzed and collected in first channel by flow cytometry (Ex./Em.= 488/ 525 nm).

Confocal Laser Scanning Microcopy (CLSM) Imaging. CLSM was chosen to investigate the cellular internalization of NFH-loaded nanoparticle by SH-SY5Y cells. SH-SY5Y cells were seeded in glass-bottom 6-well plates at a density of 1.0×10^5 cells per well in 2.0 mL of DMEM/ F12k (1:1) medium and cultured for 24 h. Then the medium was replaced with 2.0 mL fresh medium followed by an addition of 200 μL FITC labeled NFH-nBSA and TAT-NFH-nBSA nanoparticle (0.5 mg mL^{-1}). The cells were incubated at 37 ℃ for 2 h. The culture medium was removed and the cells were rinsed with cold PBS three times and fixed with 4% paraformaldehyde for 30 min at room temperature. Subsequently, the cells were treated with 0.5% Triton X-100 in ice bath for 15 min. Finally, the cells were stained with the nuclear dye DAPI as a positive control. Images of cells were acquired using a Zeiss LSM 5 Pascal confocal laser scanning microscope (Carl Zeiss AG, Oberkochen, Germany) imaging system.

Flow Cytometry Study. For flow cytometry, SH-SY5Y cells were seeded in 6-well plates at a density of 2.0×10^5 cells per well in 2.0 mL complete DMEM/F12k (1:1) medium and cultured for 24 h. Then the medium was replaced with 2.0 mL fresh medium containing 200

μL FITC-labeled NFH-nBSA and TAT-NFH-nBSA nanoparticle (0.5 mg mL^{-1}). The cells were incubated at 37 ℃ for pre-set time points, 0.25, 0.5, 1, 2 and 3 h. Thereafter, the culture medium was removed and the cells were washed with cold PBS three times and then harvested. The amount of intracellular fluorescent signal of FITC was quantified using BD Accuri™ C6 flow cytometer, indicating the amount of NFH-nBSA and TAT-NFH-nBSA nanoparticle internalized by SH-SY5Y cells.

***In Vivo* Imaging Studies.** Whole-body *in vivo* biodistribution and brain accumulation in healthy BalB/C nude mice was examined using eXplore Optix MX animal optical molecular imaging system (General Electric Company, USA) at 580 nm excitation and 692 nm emission wavelengths. Tail vein injection of Cy5.5 labeled 16.0 mg mL^{-1} (concentration of NFH) NFH-nBSA and TAT-NFH-nBSA, respectively, 200.0 μL for each mouse. Then the mice were given general anesthesia with glutaraldehyde (2%). At time points of post-injection 1, 4, 24 and 48 h, the mice were fixed with tapes and taken pictures from the back.

Pharmacokinetics Study. The pharmacokinetic properties of NFH-nBSA and TAT-NFH-nBSA nanoparticles were investigated in a healthy mouse model using KM male mice (~40 g). The NFH-nBSA and TAT-NFH-nBSA nanoparticles were injected into the tail vein intravenously at a dose of 3.0 mg kg^{-1} (concentration of BSA) with three mice in each group (n = 3). Time points selected for the nanoparticles were 0, 2, 6, 10, 24, 48, and 72 h post-injection. At specified time points, mice were sacrificed and the blood samples were collected in coagulating tubes to separate the blood cells. The samples were stored at 4 ℃ until analysis. The serum of each sample was analyzed using UV-vis. The absorbance of

each sample at 388 nm was recorded. The residual content in plasma at each time point was calculated as follows:

$$\text{Residual content (\%)} = \text{Abs}_{\text{time point}} / \text{Abs}_{0h} \times 100$$

Parkinsonian Mice Models. Wild type C57BL/6 male mice, 10 to 11 weeks old, were injected with 15 mg kg^{-1} MPTP (2.5 mg mL^{-1} in PBS) intra-peritoneally on 30 consecutive days. The treatment was carried out every 3rd day from the 6th day. The healthy mice with no treatment were set as control group. The MPTP treated mice with no drug treatment were set as PD group. The body weight of each mouse was taken and recorded each time after the injection every day. Animals were sacrificed 1 h after the behavioral tests following the last treatment on the 30th day, by cervical dislocation after bloodletting from the retinal vein plexus. The blood was collected in separation gel coagulation promoting tubes and anticoagulation tubes for routine biochemistry tests and routine blood parameters tests, respectively.

Parkinsonian Mice Behavioral Tests. Behavior was assessed for 1 h after drug administration after the final treatment on day 30th and was repeated for 3 three times. Animals were randomly assigned to control group, PD group, NFH-nBSA and TAT-NFH-nBSA treatment groups (n = 5). Control mice received PBS only and PD group received PBS and MPTP only. The treatment was administered through tail vein injection of 0.5 mg mL^{-1} NFH-nBSA and TAT-NFH-nBSA, respectively, 200.0 μL for each mouse.

Muscular Rigidity Study. In the rodent, catalepsy was characterized as a loss of independent movement ability where limbs uncharacteristically remain in fixed positions. The muscular rigidity study (maximum duration of 100 s) began by placing the forepaws of

male Parkinsonian mice (15-25 g) on a horizontal bar elevated 30.0 cm above the bench with diameter of 4.0 mm and length of 30.0 cm. The test ended when the animal came off the bar by landing on the bench. Each value represents average (± SEM) time in cataleptic state of mice per treatment group during a 100 s test session.

Bradykinesia Study. Efficacy of treatment can be reflected by reversal of akinesia. Movement was studied in an activity box (L: 24.0 cm; W: 18.0 cm; H: 14.0 cm), containing 48 equally spaced painted grids (3.0 × 3.0 cm) on the bottom. Activity was measured by counting the number of grids each mouse walking through during the observed 30 s. Each value represents the mean (± SEM) of the total number of grids crossed of n = 5 mice per treatment group during the 30 s × 3 measurement period in the behavioral test session.

Quantitative Real-Time PCR (QRT-PCR). For isolation of total RNA, frozen SNpc was homogenized in 800 µL Trizol (Life Technologies, USA) according to the manufacturer's instructions for 20 s using an Ultra-Turrax (IKA, Staufen, Germany) and incubated for 5 min at room temperature. Extracts were mixed with 160.0 µL chloroform, incubated for 3 min and centrifuged for 15 min at 12,000 × g (4 ℃). The top clear phase was mixed with 500.0 µL 75% ethanol, transferred to columns of the SV Total RNA Isolation System (Promega, Mannheim, Germany) and preceded according to the manual. RNA was eluted in 60 µL nuclease-free water and the concentration was measured spectrophotometrically (Infinite® 200 NanoQuant, Tecan, Crailsheim, Germany). Isolated SNpc RNA was reverse-transcribed into cDNA using the QuantiTect® Reverse Transcription Kit (Qiagen; Hilden, Germany). Primer3 algorithm (SDSC Biology Workbench, San Diego, CA, USA) was used to design the primer sequences: GGTCTACTGTCTGCCCGTGAT and

CAATGTCCTGGGAGAACTGG for tyrosine hydroxylase (TH), TTCTCCCTTGGCGTTGGGTTTG and AGAAGCTCGTCAGGGAGTTAA for dopamine transporter (DAT). QRT-PCR was accomplished with Sensimix SYBR NoRox (Bioline, Luckenwalde, Germany) on 96-well format (Mastercycler® ep realplex epgradient S, Eppendorf, Hamburg, Germany). Gene expression levels of the samples were calculated from a standard curve generated from pooled cDNA of all samples (n = 6) and diluted by 2n in 8 steps. Sample cDNA was diluted 1:50 and measured in triplicates. Standards were measured in duplicates.

Western Blotting Analysis. Proteins were isolated from SNpc using a cell lysis buffer kit (Cell Signaling, USA). 10% SDS-PAGE was used to analyze amples (n = 4) containing equal amounts of protein (20 μg) and then transferred them onto a polyvinylidene difluoride (PVDF) membrane (Immobilon, Millipore, USA). After blocking with 5% fat-free milk in tris-buffered saline and Tween 20 (TBST), the membranes were probed overnight at 4 ℃ with a rabbit polyclonal antibody against TH (1:1000 dilution, ab112, Abcam, USA) and GAPDH (1:2000 dilution, Boster, China). After incubation for 2 h at room temperature in a 0.5% BSA TBST solution containing horseradish peroxidase (HRP)-conjugated secondary antibodies (1:2000 dilution, Jackson, USA), the immunoblots were then treated with an ECL reagent. The results were analyzed using OdysseyFc Imaging System (MS Technosystems, Osaka, Japan).

H&E Staining and Immunohistochemical Analysis. After the animals were sacrificed, the tissues (hearts, livers, spleens, lungs and kidneys) and SNpc in brains were removed and cut into small pieces, fixed in 4% paraformaldehyde for 8 h. Then the tissues were embedded

in paraffin and cut into 5 μm sections and placed on poly-L-lysine-coated slides for hematoxylin and eosin (H&E) staining and immunohistochemical analysis, respectively. Duplicate slices were placed on glass microscope slides and stained for histopathological analysis. Every second section was processed for immunohistochemistry. For proper identification of the SNpc, all sections were incubated with polyclonal rabbit anti-TH (1:2000 dilution, ab112, Abcam, USA). Typically, the sections were treated with 3% hydrogen peroxide aqueous solution for 15 min to quench endogenous peroxidase activity, and then heated to boiling in EDTA antigen retrieval solution for 10 min in water bath for antigen retrieval. Then the sections were allowed to cool down, rinsed with PBS three times. Subsequently, the sections were treated with goat serum in TBS for 20 min to block non-specific binding sites, followed by incubation with TH antibody for 1 h at room temperature. Then, the sections were rinsed with PBS three times, incubated with goat anti-mouse HRP secondary antibody (1:1000) followed by colorimetric detection with diaminobenzidine (DAB) as chromogen. Finally, the sections were counterstained with hematoxylin and prepared for mounting. The images were taken by using a Nikon ECLIPSE Ti microscope.

Statistical Analysis. The results were analyzed using the Tukey's honestly significant difference test for multiple comparisons followed by John Wilder Tukey's test to identify significant differences between groups. Family-wise significance and confidence level was $p<0.05$. All results were expressed as means ± standard error of the mean (SEM).

RESULTS AND DISCUSSION

Preparation and Characterization of Protein-Based Zwitterionic Nanoparticles for Iron Chelation Therapy. High-efficiency chelation of excess Fe ions in brain is an effective modality to decrease the loss of dopaminergic neurons and difficulties of motor control in PD. Therefore, we constructed a long-circulating therapeutic system with Fe chelator NFH-loaded TAT-NFH-nBSA to enable the Fe chelation inside brain. In our delivery system, zwitterionic polymer PMPC with excellent non-fouling property was selected to prolong the *in vivo* life time and properly shield from the chelation during blood circulation. TAT can endow the nanoparticles enhanced BBB permeability, and the concentration and retention time of the loaded therapeutics inside brain can be improved as well. Fig. 1 illustrates the structure and synthesis procedure of TAT-NFH-nBSA for PD treatment and the details are described in Experimental Section. In the present work, we used BSA as a single-sized core to guarantee the ultra-small size and uniform size distribution. In addition, BSA is just a model protein, which can be replaced by any other kind of active proteins to endow the nanoparticles with various extra treatment capacities. Firstly, double bonds can be modified on the surface of BSA after acrylation. Zwitterionic polymer PMPC shell was then constructed on the surface of acrylated BSA (aBSA) core through *in-situ* free radical polymerization. As a family member of cell-penetrating peptides (CPPs), TAT was finally conjugated into the delivery system through the amidation reaction with carboxyl group in monomer acrylic acid introduced *via* polymerization. We used ^{31}P NMR to confirm the encapsulation of PMPC on the surface of the nanoparticles. As shown in Fig. 2a, the peak of MPC is at 0.57 ppm and BSA shows no peak. The successful attachment of PMPC out layer in the nanoparticles is confirmed by the presence of a new signal of PMPC-modified

nanoparticles (nBSA) at 0.40 ppm, compared with the ^{31}P NMR results of MPC and BSA. In addition, the ICP-AES results show that the concentration of Fe decreases from 8.57% in purchased hemin-Cl (agrees with the calculated value) to 0.013% in NFH (Table 1), which demonstrates that the Fe is already removed from the core of the purchased hemin-Cl. Meanwhile, the loading of NFH on the nanoparticles can be further confirmed by UV-vis spectrometer (Fig. 2d). NFH shows a red-shift to 388 nm in the UV-vis spectroscopy compared with purchased hemin-Cl at 382nm. The red-shift of NFH can attribute to the removal of Fe in the porphyrin ring of purchased hemin-Cl. Furthermore, UV-vis absorption spectra of NFH-nBSA and TAT-NFH-nBSA nanoparticles also show the characteristic absorption peak of NFH at 388 nm, which demonstrates the successful loading of NFH on the nanoparticles.

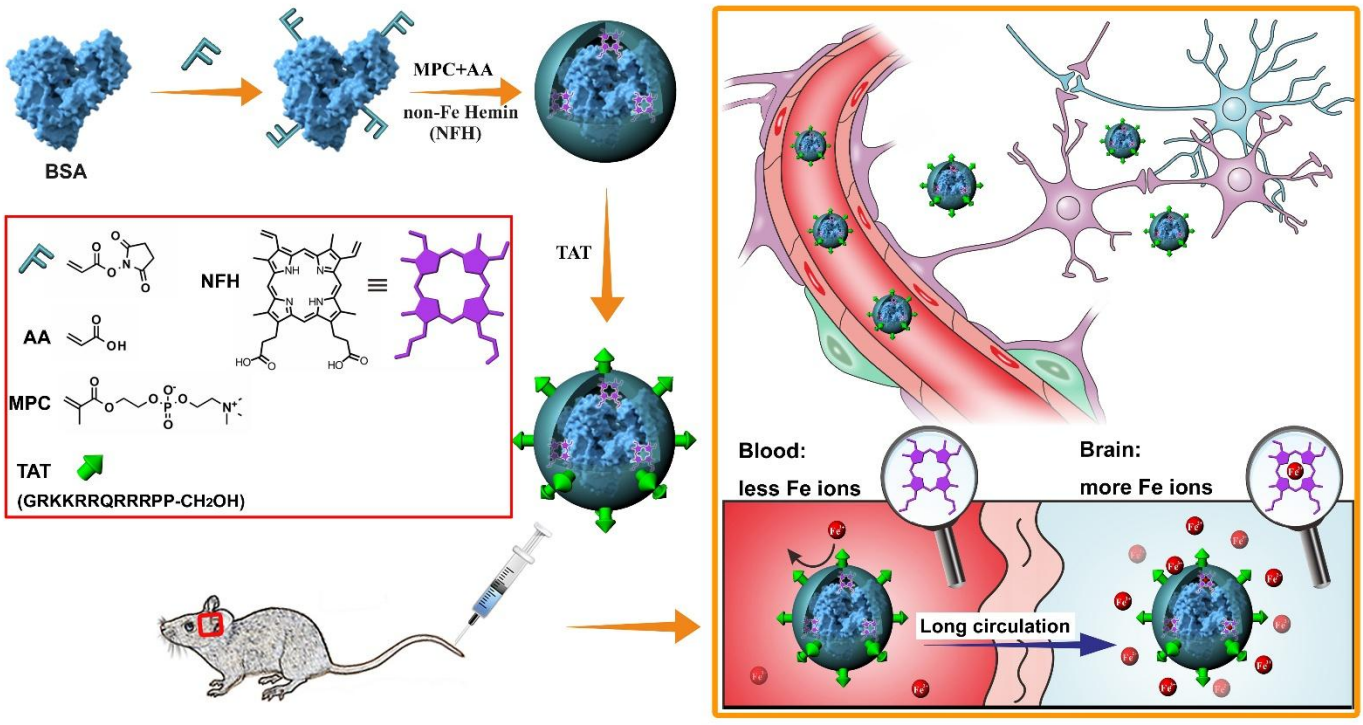

Figure 1. Synthesis of the TAT-NFH-nBSA nanoparticle for the treatment of Parkinson's disease and the schematic diagram of the protective hydration layer of PMPC for delayed saturation. The non-

fouling layer of PMPC on the surface can endow the iron chelation nanoparticles TAT-NFH-nBSA long *in vivo* blood circulation life time after tail vein injection. Furthermore, the chelation with various free ions in plasma can be greatly prevented by this protective layer at the same time to give a delayed saturation feature during the blood circulation. With the assistance of BBB-permeable ligand TAT, the nanoparticles can target the brain and then the iron chelation therapy for PD can be achieved.

To confirm the successful bioconjugation of TAT, TAT was labeled with FITC, and the fluorescence of the non-TAT-modified nanoparticles (NFH-nBSA) and TAT-modified nanoparticles (TAT-NFH-nBSA) were collected with flow cytometer. As shown in Fig. 2b and 2c, TAT-NFH-nBSA nanoparticles show extra FITC fluorescence signal (Fig. 2c) compared with NFH-nBSA nanoparticles (Fig. 2b). Therefore, the attachment of TAT peptides on the surface of the drug delivery system can be confirmed.

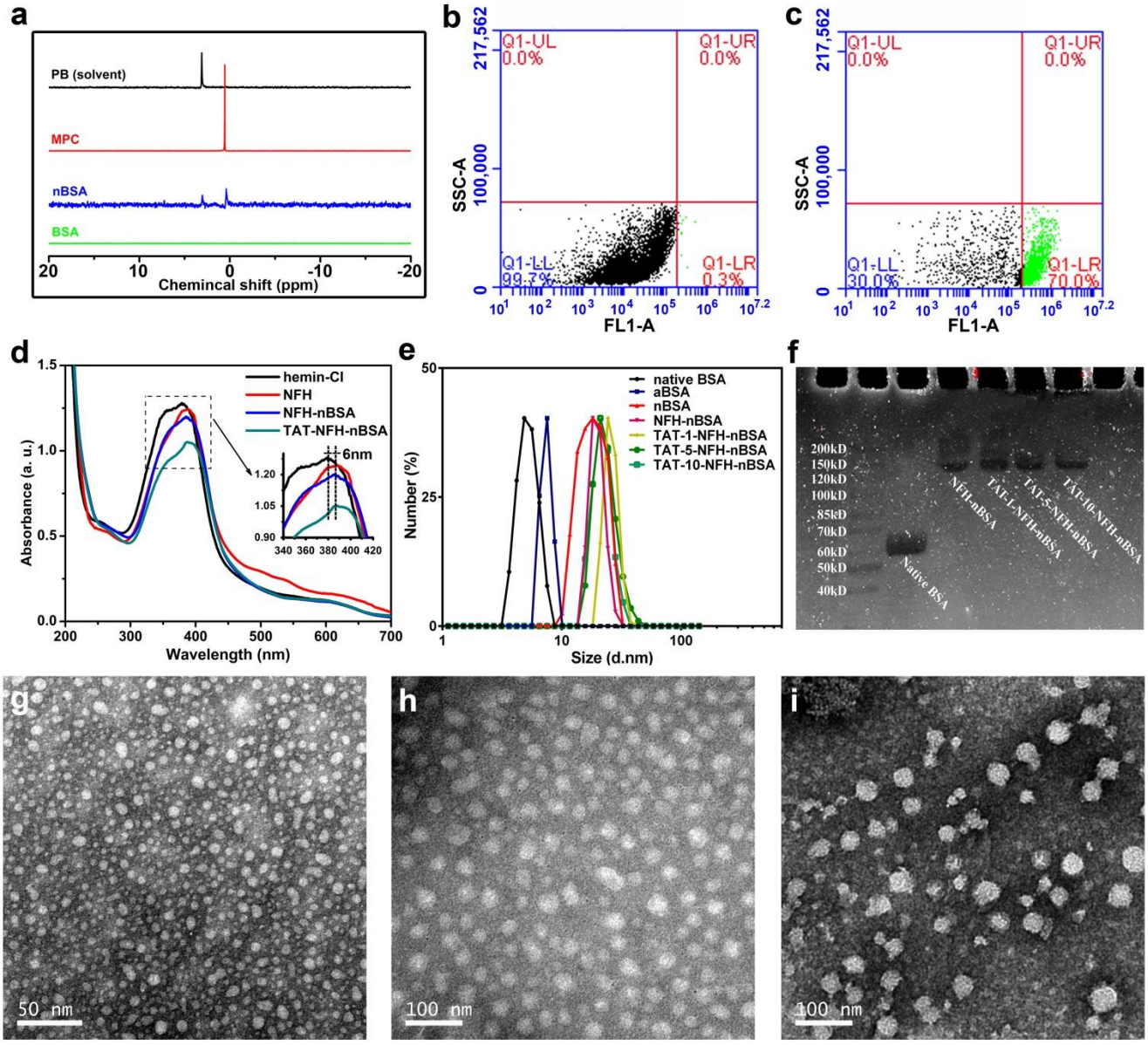

Figure 2. Characterization of drug-loaded delivery system. (a) ^{31}P NMR of phosphate buffer (PB, 20 mM, pH 7.4), MPC monomer, nBSA nanoparticles (0.5 mg mL^{-1} in PB), aBSA (0.5 mg mL^{-1} in PB) in 50% H_2O/50% D_2O. Flow cytometry of the nanoparticles, signal of FITC was collected form FL1 channel, 10,000 particles were recorded and analyzed (b, c). NFH-nBSA (b), and FITC-labeled TAT-NFH-nBSA (c). (d) UV-vis spectra of purchased hemin-Cl, NFH-nBSA and TAT-NFH-nBSA in 50% H_2O/50% DMSO. (e) The hydrodynamic sizes of native BSA, aBSA, nBSA, NFH-nBSA, TAT-1-NFH-nBSA, TAT-5-NFH-nBSA and TAT-10-NFH-nBSA nanoparticles. (f) The SDS-PAGE results of native BSA, NFH-nBSA, TAT-1-NFH-nBSA, TAT-5-NFH-nBSA and TAT-10-NFH-nBSA nanoparticles. (g-i) The TEM images of native BSA, NFH-nBSA, TAT-1-NFH-nBSA nanoparticles.

To further explore the BBB penetration ability and treatment effect for PD, a series of TAT-modified nanoparticles were prepared (TAT-1-NFH-nBSA, TAT-5-NFH-nBSA and TAT-10-NFH-nBSA, the number stands for the molar ratio of TAT to BSA). The molecular weight (MW) of the different drug delivery systems was characterized by SDS-PAGE (Fig. 2f). The MW of native BSA is around 65 kD, and the MW of NFH-nBSA and TAT-NFH-nBSA increases to around 150 kD after modification. The size and surface properties of the nanoparticles have significance influence on the *in vivo* circulation behaviors. Thus, the parameters including size, size distribution and zeta potential of the nanoparticles were analyzed with the use of DLS. As shown in Table 2, native BSA, aBSA, nBSA, NFH-nBSA and TAT-NFH-nBSA are different in size but similar in zeta potential, near 0 mV and a slight negatively charged. The sizes of the TAT-modified nanoparticles are around 24 nm, as shown in Fig. 2e. As shown in the TEM images (Fig. 2g-i), native BSA, NFH-nBSA and TAT-NFH-nBSA exhibit uniform spherical morphology and well-defined size distributions with sizes corresponding to the results in DLS. No significant changes in the morphology are observed after the surface modifications. As determined by UV-vis, the NFH loading ratio of the nanoparticles is 17.6%, which is 0.12 mg mL^{-1} (the concentration of BSA was 0.5 mg mL^{-1}).

Table 1. ICP-AES Results of Iron Chelator

Sample	Fe contained (%)
Purchased hemin-Cl	8.57
NFH	0.013

Table 2. DLS Parameters of Different Systems

Systems	d (nm)	ξ (mV)
Native BSA	5.23 ± 1.01	-10.01
aBSA	7.33 ± 0.75	-8.11
nBSA	18.27 ± 6.79	-7.07
NFH-nBSA	19.61 ± 2.91	-4.46
TAT-1-NFH-nBSA	26.01 ± 3.47	-4.95
TAT-5-NFH-nBSA	24.36 ± 4.33	-4.74
TAT-10-NFH-nBSA	23.40 ± 5.31	-4.36

Diameters (d) and zeta potentials (ζ) were all measured by DLS. The dispersed phase is 20 mM phosphate buffer, pH = 7.4.

***In Vitro* Chelating Ability.** To verify the Fe chelating effect and the saturation feature of these four different drug delivery systems in the blood circulation condition, the ferrozine method was applied. After binding with Fe^{2+}, a colored ferrozine complex with emission at 562 nm will generate. The addition of NFH-loaded nanoparticles can compete with ferrozine in chelation with Fe^{2+}, so that the generated Fe^{2+}-ferrozine complex will present an inverse relationship with the concentration of the added nanoparticles. After the binding between chelating agent and iron ions, Fe^{2+} will be quickly autoxidized to the corresponding Fe^{3+} compounds, so that this method actually reflects the overall iron ions chelating ability rather than either of them. It's our hypothesis that with the protection of PMPC out layer on the surface of NFH-loaded BSA, the Fe chelating effect within a certain period of time will

decrease to some extent and the saturation state will be delayed obviously. With the use of ICP-AES, the free Fe ions in the serum of the C57BL/6 mouse, the animal model used in the *in vivo* treatment studies, were analyzed to be 1.96 ± 0.18 μM. So that the concentration of Fe ions in the chelating assays was chosen to be 2 μM and 15 μM to mimic the condition in blood circulation, and the chelating duration between the nanoparticles and Fe^{2+} was chosen to be 30 min. As shown in Fig. 3a and 3b, no matter for the low concentration or high concentration of Fe^{2+}, free NFH shows the strongest iron chelating ability and much higher than the other four modified groups. Because of the protective property of the PMPC out layer, the contact between the free Fe^{2+} in the solution and the NFH loaded inside the PMPC polymer layer will be greatly hindered. Therefore, during the observed duration, the ion chelating effect of the MPC encapsulated nanoparticles is much lower than the free NFH. In addition, compared with the TAT-modified groups, the non-TAT-modified nanoparticles show the lowest chelating potency which should be due to the compact hydration layer around the MPC surface. The introduction of TAT on the surface of the nanoparticles affects the density of the hydration layer thus further affect the ion chelating potency as well. The calculated saturation state of each nanoparticle under different conditions is summarized in Fig. 3c and 3d. The standard group stands for the theoretical value under each condition. It's the ideal degree of saturation of NFH when all the free Fe^{2+} ions in the solution are bound or the entire added NFH has chelated with Fe^{2+} ions. From the results shown in Fig. 3c and 3d, we can clearly see that with the protection of PMPC out layer on the surface, the saturation state is delayed greatly under both Fe^{2+} concentration conditions. Therefore we can suppose that our original hypothesis for chelating effect is reliable, which means that

this kind of structure of the iron chelator system indeed possesses a delayed saturation feature in blood circulation.

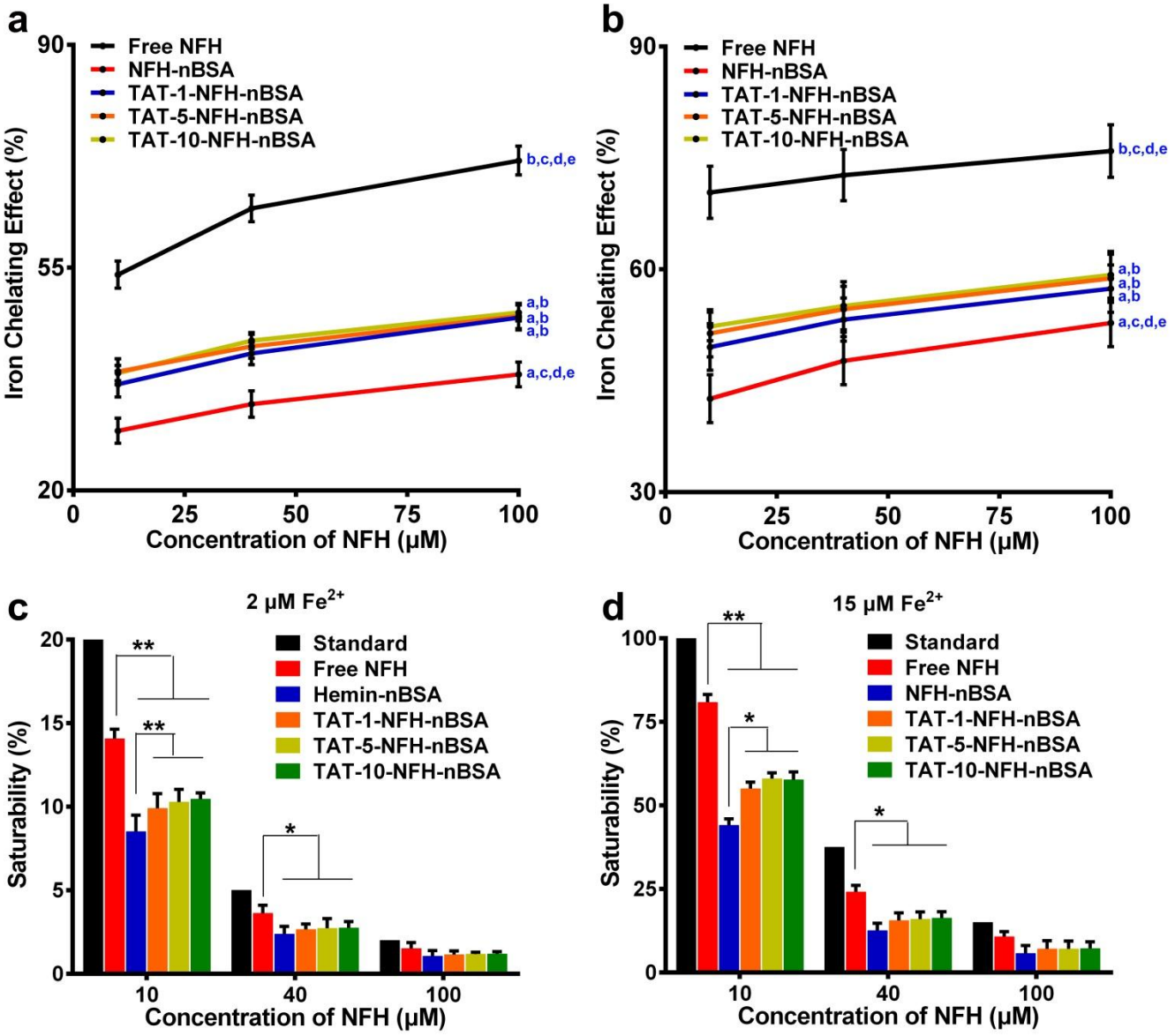

Figure 3. ***In vitro*** **chelate ability of the TAT-NFH-nBSA nanoparticle.** (a, b) Iron-chelating effect of 10, 40, 100 μM free NFH, NFH-nBSA and TAT-NFH-nBSA nanoparticles with 2 μM (a) & 15 μM (b) $FeSO_4$ in pH 6.9 ammonium acetate buffer for 30 min. [a]$p<0.05$ *vs.* Free NFH, [b]$p<0.05$ *vs.* NFH-nBSA, [c]$p<0.05$ *vs.* TAT-1-NFH-nBSA, [d]$p<0.05$ *vs.* TAT-5-NFH-nBSA, [e]$p<0.05$ *vs.* TAT-10-NFH-nBSA. (c, d) Saturability of 10, 40, 100 μM free NFH, NFH-nBSA and TAT-NFH-nBSA nanoparticles with 2 μM (c) & 15 μM (d) $FeSO_4$ in pH 6.9 ammonium acetate buffer for 30 min. **$p<0.01$, *$p<0.05$.

Biocompatibility and Cell Uptake of the TAT-NFH-nBSA Nanoparticles. The biocompatibility and cytotoxicity of the materials are important for the biomedicine used *in vivo*. Here, we used MTT assay to examine the cell viability after co-cultured with the nanoparticles. As shown in Fig. 4a, a high cell viability can be observed after the incubation of SH-SY5Y cells with free NFH, NFH-nBSA and TAT-NFH-nBSA nanoparticles for 24 h, even with an extremely high concentration of NFH (192.5 μM). From the MTT results, the low cytotoxicity of these nanoparticles *in vitro* can be proved.

To gain quantitative result of the cell uptake ability of these four different drug delivery systems, flow cytometry analysis was performed to measure the uptake amount of FITC labeled NFH-nBSA and TAT-NFH-nBSA nanoparticles. As shown in Fig. 4d, the cell internalization ability by SH-SY5Y cells for three TAT-NFH-nBSA groups increases tremendously as the incubation time prolongs, which indicates that TAT-NFH-nBSA nanoparticles can be easily internalized by SH-SY5Y cells. What's more, among these three different TAT labeled groups, the TAT-10-NFH-nBSA shows the greatest ability (50.31% at 3 h) uptaken by the cells than the other two TAT labeled nanoparticles (30.48% for TAT-5-NFH-nBSA and 17.2% for TAT-1-NFH-nBSA at 3 h). While the internalization of NFH-nBSA by cells barely changes during the observed 3 h which is only 2.4% of the initial dose. The flow cytometry analysis results demonstrate that the modification of TAT peptide on the surface of nanoparticles could improve the cell uptake ability significantly and the internalization ability is proportional to the amount of TAT modified. The enhanced cell uptake of TAT-NFH-nBSA nanoparticles is beneficial for improving the drug delivery efficiency in CNS. The CLSM observation (Fig. 4e) also confirms the results collected by

flow cytometer. After incubation for 2 h, a little amount of NFH-nBSA nanoparticles is observed in SH-SY5Y cells and localize in the cytoplasm. In contrast, TAT-modified nanoparticles show greater ability entering the cells. Compared with TAT-5-NFH-nBSA and TAT-10-NFH-nBSA nanoparticles, TAT-1-NFH-nBSA nanoparticles localize mostly in the cytoplasm with little in the nucleus. On the contrary, more TAT labeled groups (TAT-5-NFH-nBSA and TAT-10-NFH-nBSA group) appear both in the cytoplasm and the nucleus. In short, the labeling of TAT peptide on the surface of nanoparticles can improve their cell internalization ability significantly.

The *in vitro* anti-Parkinson efficacy of NFH-nBSA and TAT-NFH-nBSA nanoparticles is the basis for using *in vivo*. The treatment effect *in vitro* was evaluated against MPTP treated SH-SY5Y cells (named as PD cells) using MTT assay and flow cytometry, employing free NFH as control (Fig. 4b and 4c). As shown in Fig. 4b, TAT-NFH-nBSA nanoparticles show similar cell viability as free NFH against the PD cells in each concentration. However, the NFH-nBSA group displays barely no extral anti-Parkinson efficacy as concentration increases. The low efficacy of NFH-nBSA group might in part be due to the protective property of the PMPC polymer shell. The NFH-nBSA nanoparticles could not be largly internalized by the cells as the TAT-NFH-nBSA groups do. Besides, because of the slight cytotoxicity at higher concentration, free NFH and TAT-NFH-nBSA groups show the greatest efficacy around the concentration of 48.1 μM, which is selected as the single concentration for the *in vitro* ROS level reversing effects assay.

The ROS level of PD cells induced by MPTP for 24 h was determined by ROS kit and recorded with flow cytometer. The untreated PD cells and healthy cells were used as controls.

As shown in Fig. 4c, the NFH-nBSA treated cells don't show significant ROS decreasement compared with the PD cells. However, TAT-NFH-nBSA nanoparticles prompt an obvious reduction of ROS in comparison to the PD group and even approach to the level of healthy cells. From these two kinds of *in vitro* anti-Parkinson assays, it can be concluded that TAT-NFH-nBSA exhibits much more remarkable neuroprotective ability than the NFH-nBSA group, no matter in reversing the ROS level or promoting the cell viability of PD cells.

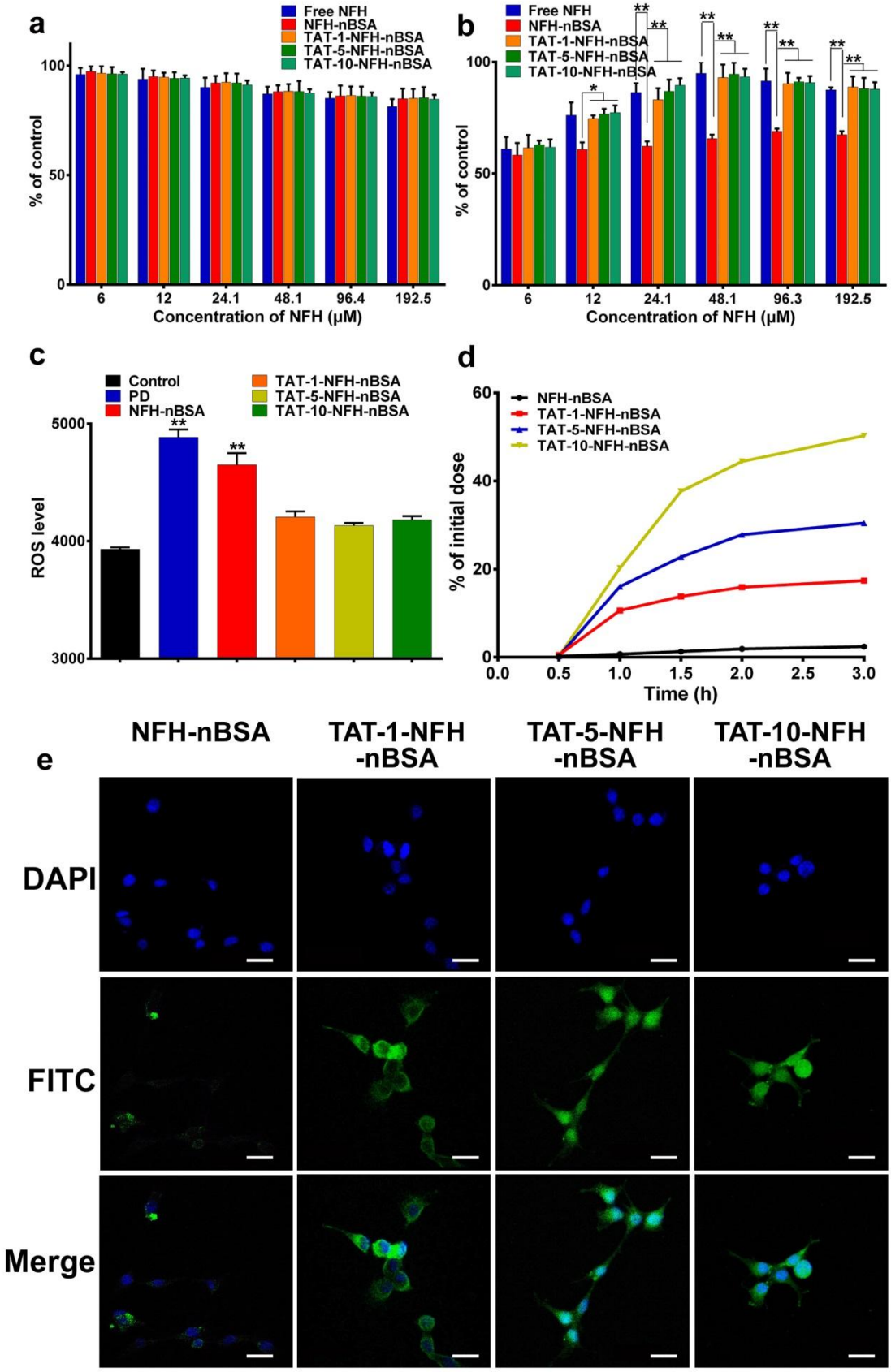

Figure 4. Biocompatibility and cell uptake of TAT-NFH-nBSA nanoparticles. (a) 24 h cell viability of free NFH, NFH-nBSA and TAT-NFH-nBSA nanoparticles to SH-SY5Y cell lines determined by MTT assay, repectively. (b) *In vitro* 48 h anti-Parkinson effects of free NFH, NFH-nBSA and TAT-NFH-nBSA

nanoparticles determined by MTT assay, respectively. **p<0.01, *p<0.05. (c) *In vitro* 24 h anti-Parkinson effects of free NFH, NFH-nBSA and TAT-NFH-nBSA nanoparticles determined by intracellular ROS level, respectively. **p<0.01 *vs.* control. (d) Flow cytometric result of SH-SY5Y cells incubated with NFH-nBSA and TAT-NFH-nBSA nanoparticles at different time intervals. (e) Confocal images of SH-SY5Y cells treated for 2 h. Blue represented FL of DAPI, the nucleus, and green represented FL of nanoparticles, scale bar is 25 μm.

***In Vivo* Pharmacokinetics and Biodistribution of NFH-nBSA and TAT-NFH-nBSA Nanoparticles.** Learning from successful strategies for the treatment of tumors in other parts of the body, prolonged circulation time of the delivery system is always able to enhance tumor targeting and accumulation.[63,64] It seems to indicate that the circulation time of the delivery systems may play a key role in the BBB penetration.[65-67] Compared with free small-molecule drugs and non-zwitterionic polymer capsulated nanoparticles, PMPC-shelled nanoparticles usually show longer blood circulation time *in vivo*.[51-55] Consequently, coating with PMPC will endow the BBB delivery shuttles stealth property and therefore much longer circulation-life time *in vivo* with better chance to contact with and penetrate through the BBB cell membrane. To evaluate the *in vivo* life time and biodistribution of the synthesized nanoparticles, Cy5.5, a near infrared fluorescence (NIRF) dye, was labeled onto the nanoparticles to show their behavior *in vivo*. Cy5.5 labeled NFH-nBSA and TAT-NFH-nBSA nanoparticles were intravenously injected via tail vein into the healthy nude mice. Subsequently, the real-time imaging of the nanoparticles *in vivo* was monitored over the time window of 48 h (Fig. 5a). After 1 h, the signals of Cy5.5 in the whole body for both NFH-nBSA and TAT-NFH-nBSA mainly locate in the brain and spine. However, for NFH-nBSA group, after 4 h, the signals in the whole body are extremely weak including the brain

and spine, indicating that NFH-nBSA nanoparticles have been quickly cleared from the CNS. We suspect that because of the gap of BBB, the non-TAT-modified group NFH-nBSA could cross BBB *in vivo* at the first 1 h time window, but would soon be recognized by the P-glycoproteins on the cells membranes of BBB and pumped back to the blood circulation. On the other hand, the signals of Cy5.5 labeled TAT-NFH-nBSA nanoparticles remain in the brain for even 48 h. Due to the existence of TAT peptides on the surface of the nanoparticles, the drug delivery system could greatly penetrate BBB and remain inside the brain for even 48 h. These *in vivo* results strongly demonstrate the critical role of TAT peptide in assisting the BBB penetration of the drug delivery system. The *in vivo* pharmacokinetics study of NFH-nBSA and TAT-NFH-nBSA nanoparticles was carried out with KM male mice. As shown in Fig. 5b, because of the great non-fouling property of MPC, the *in vivo* half-life of these four different systems can be prolonged to about 20 h.

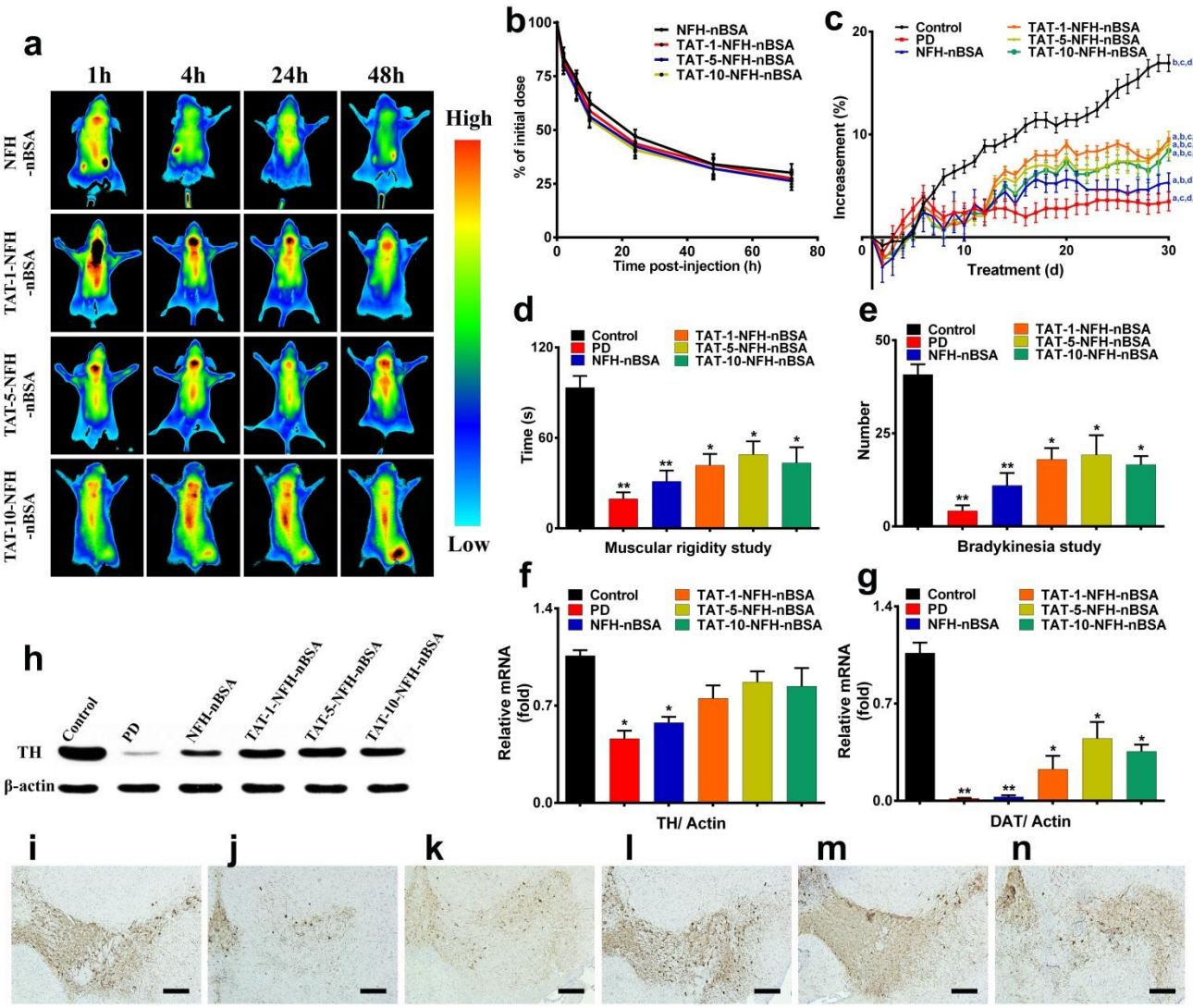

Figure 5. ***In vivo*** **pharmacokinetics and biodistribution of NFH-nBSA and TAT-NFH-nBSA nanoparticles.** (a) *In vivo* non-invasive NIRF images of time-dependent whole body imaging of healthy nude mice after intravenous injection of Cy5.5 labeled NFH-nBSA, TAT-NFH-nBSA nanoparticles for 1, 4, 24 and 48 h. (b) *In vivo* pharmacokinetics study of NFH-nBSA, TAT-NFH-nBSA nanoparticles for 72 h. *In vivo* anti Parkinson activity. (c) Body weight changes of Parkinsonian mice during the 30-day evaluation period of treatment with PBS, NFH-nBSA and TAT-NFH-nBSA nanoparticles. [a]$p<0.05$ *vs.* control, [b]$p<0.05$ *vs.* PD, [c]$p<0.05$ *vs.* NFH-nBSA, [d]$p<0.05$ *vs.* TAT-1-NFH-nBSA, [e]$p<0.05$ *vs.* TAT-5-NFH-nBSA, [f]$p<0.05$ *vs.* TAT-10-NFH-nBSA. (d) Mean duration of time for the Parkinsonian mice hanging on the bar after treatment with PBS, NFH-nBSA and TAT-NFH-nBSA nanoparticles. **$p<0.01$ *vs.* control, *$p<0.05$ *vs.* control. (e) Mean number of grids for the Parkinsonian mice creeping during the observed 30 s after treatment with PBS, NFH-nBSA and TAT-NFH-nBSA nanoparticles. **$p<0.01$ *vs.* control, *$p<0.05$ *vs.* control. The QRT-PCR results of TH (f) and DAT (g) after treatment with PBS, NFH-nBSA and TAT-NFH-nBSA nanoparticles. **$p<0.01$ *vs.* control, *$p<0.05$ *vs.* control. (h) The expression levels of TH in SNpc of the Parkinsonian mice after treatment with PBS, NFH-nBSA and TAT-NFH-nBSA nanoparticles,

determined by western blot analysis. β-Actin was the loading control. Data represent five individual experiments. Each experiment group was repeated three times. The immunohistochemical study for TH of control (i), PD (j), NFH-nBSA (k), TAT-1-NFH-nBSA (l), TAT-5-NFH-nBSA (m) and TAT-10-NFH-nBSA (n) groups, respectively. Scale bare is 200 μm.

***In Vivo* PD Treatment Efficacy of the TAT-NFH-nBAS Nanoparticles.** The *in vivo* anti-Parkinson activities were investigated using MPTP-induced Parkinsonian mice. It has been proved that MPTP can exaggerate the iron accumulation of treated mice in SNpc and MPTP-treated PD animal models have been widely used to evaluate the efficacy of iron chelators.[15,17,21,22,26,37] The mice were divided into six groups (n = 5) randomly. After five-day continuous intraperitoneal injection of MPTP, the mice began to show the symptoms of Parkinson and drops of body weight, then the treatment started. The mice in different treatment groups were intravenously injected *via* the tail vein with PBS, NFH-nBSA and TAT-NFH-nBSA nanoparticles at a NFH dose of 1.2 mg kg^{-1} once every 3 days, respectively. The body weights of mice treated with different groups were examined every day (Fig. 5c). Compared with the Parkinsonian mice, the groups treated with TAT-NFH-nBSA nanoparticles gain much more increasement in body weight. However, in NFH-nBSA treated group, the body weight increases slowly, espectively during the last 10 days.

As shown in Fig. 5d and 5e, the Parkinsonian symptoms are remarkably reversed by the treatment with the three different amount of TAT-conjugated TAT-NFH-nBSA nanoparticles and approaching the results of the healthy group. In the muscular rigidity studies, the hanging durations are 93.4 s for healthy group, 19.6 s for PD group, 31.2 s for NFH-nBSA group, 41.8 s for TAT-1-NFH-nBSA group, 49.0 s for TAT-5-NFH-nBSA and 43.4 s for TAT-10-NFH-nBSA, respectively (as shown in Fig. 5d). While in the bradykinesia

studies, the number of grids mice crept during the observed 30 s is 40.8 for healthy group, 4.2 for PD group, 11.0 for NFH-nBSA group, 18.0 for TAT-1-NFH-nBSA group, 19.2 for TAT-5-NFH-nBSA group and 16.6 for TAT-10-NFH-nBSA group, respectively. Remarkably, in both behavioral tests, TAT-5-NFH-nBSA nanoparticles exhibit significant Parkinsonian behavioral reversion efficacy in Parkinsonian mice and better than the other TAT-conjugated groups (Movie 1-6).

In addition to the improvement of behavior, changes of physiological indexes are worthy of attention as well. TH is the speed-limiting enzyme of the bio-synthesis of DA inside brain and also a marker for dopaminergic neurons.[2,10,12] TH is not only acting as a secondary factor to cause a series of abnormalities in PD, but also can be deactivated by ROS at the same time.[2] Therefore TH might be an important primary factor directly involved in the PD pathogenesis. DAT located in the presynaptic membrane of dopaminergic neurons could regulate the concentration of DA in the synaptic cleft. The number of DAT can indirectly reflect the function of dopaminergic neurons in SNpc and thus DAT is regarded as a marker of dopaminergic neurons. To verify whether the amount of TH and DAT has been altered by the treatment, the QRT-PCR, western blot analysis and immunohistochemical method were used to examine the expression of mRNA, proteins and positive neurons of TH and DAT.

From the QRT-PCR results shown in Fig. 5f and 5g, the TAT-5-NFH-nBSA group shows the most noteworthy promotion of both mRNA level of TH and DAT compared to the PD group. Similar with the results of behavioral tests, NFH-nBSA group shows barely any extra reversion of Parkinsonian symptoms in comparison with the non-treated PD mice group. As

shown in Fig. 5h, the western blot data reveal that TH protein expression is down-regulated greatly in Parkinsonian mice in comparison with untreated healthy control, whereas the expression of TH protein is notably enhanced by TAT-NFH-nBSA nanoparticles compared to the PD group. However, the expression level of TH protein of NFH-nBSA treated mice is slightly increased on the basis of PD group (Fig. 5h). As shown in Fig. 5i-n, the treatment with NFH-loaded drug delivery systems prevents the development of motor deficits caused by MPTP administration and significantly protects the dopaminergic neurons in the SNpc, as assessed by quantification of TH proteins shown in Fig. 5f and the labeled dopaminergic neurons in Fig. 5i-n. The immunohistochemistry on striatal slices demonstrates the neuron protective effects of TAT-NFH-nBSA nanoparticles. These results together clearly indicate that the TAT conjugated nanoparticles, especially the TAT-5-NFH-nBSA group, can be an effective modality to reverse the Parkinsonian symptoms, no matter in behavior, protein level, mRNA level or the number of alive dopaminergic neurons.

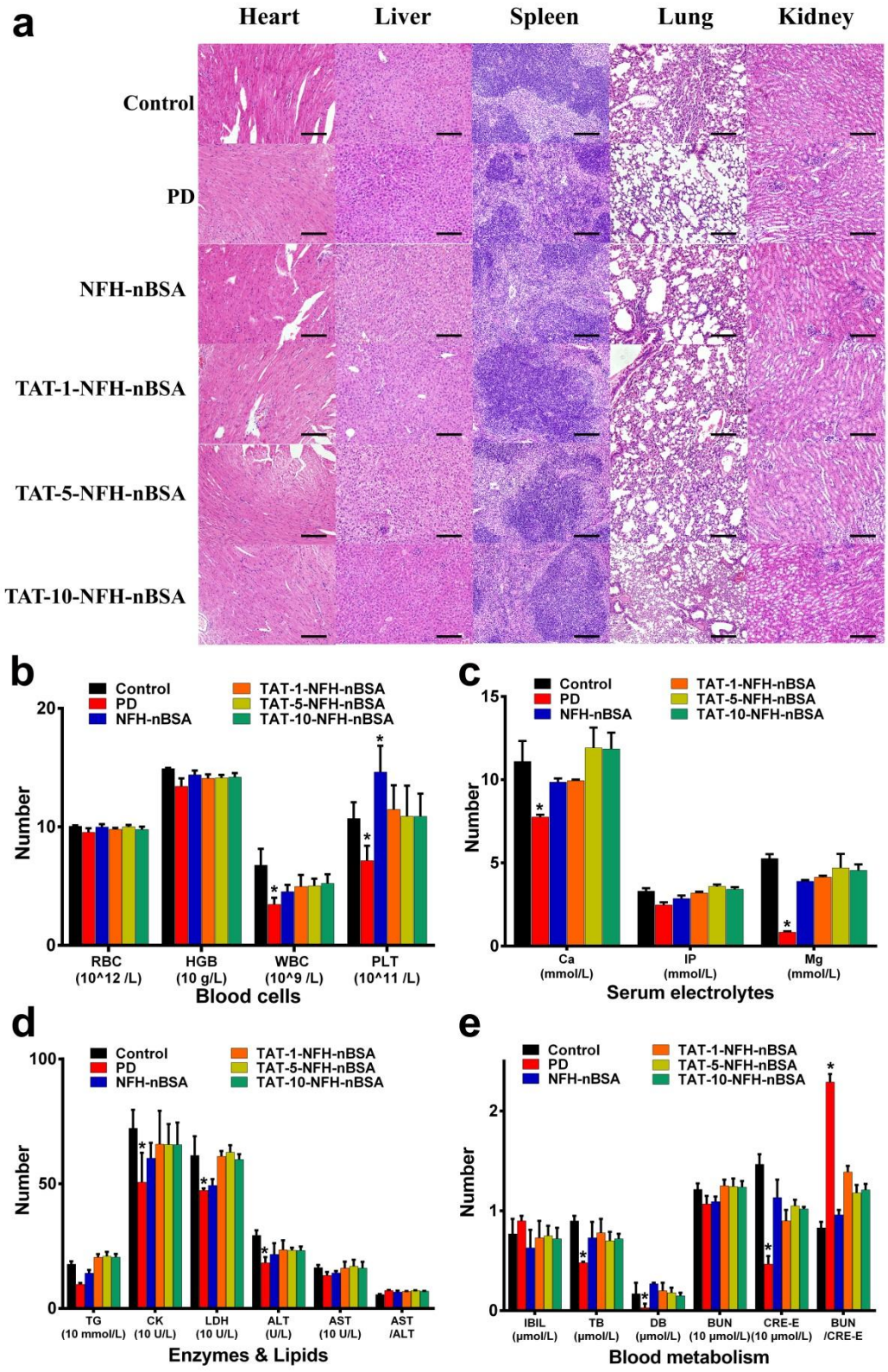

Figure 6. ***In vivo*** **toxicity evaluation of the different drug delivery systems.** (a) Organs including hearts, livers, spleens, lungs and kidneys were sectioned and stained with H&E, scale bar is 100 μm. (b) The parameters of blood routine tests of the treated PD mice. *p<0.05 *vs.* control. (c-e) Biochemical indexes of the treated PD mice, (c) serum electrolytes; (d) enzymes and lipids; (e) blood metabolisms. *p<0.05 *vs.* control.

***In Vivo* Toxicity Evaluation of the TAT-NFH-nBSA Nanoparticles.** *In vivo* toxicity evaluation of these four different drug delivery systems was performed on PD mice models after treatment for 30 days. The delivery systems were injected *via* the tail vein once every 3 days for 24 days (total eight injections). Both control group and PD group only received PBS. Histological analysis can show a detailed visual microscopic evaluation and histological assessment of inflammation caused by the injected nanoparticles and indirectly declares the therapeutic effects of these delivery systems. No obvious histopathological abnormalities or lesions can be found in heart, liver, spleen, lung and kidney (Fig. 6a). The H&E staining images show the same properties as those of healthy mice. However, obvious pathological change can be observed in the lung for PD mice and slight changes for NFH-nBSA treated PD mice.

In order to detect more detailed physical and chemical indicators, blood was collected from the mice, kept in separation gel coagulation promoting tubes and anticoagulation tubes for routine biochemistry tests and routine blood parameters tests, respectively. MPTP can damage dopaminergic neurons in SNpc and cause similar symptoms of PD. It may also induce series of inflammatory responses, which would be indicated by changes in number of blood cells and differences in the level of the biochemical indexes in serum. Consequently, blood routine examination and biochemical parameters test were performed. For the blood routine tests, we had selected important accounts of red blood cell (RBC), hemoglobin (HBG), white blood cell (WBC) and platelets (PLT). Complete blood count (CBC) for healthy mice and PD groups was performed as positive and negative controls. Compared with the control group, the results of three TAT-NFH-nBSA groups do not suggest any acute

toxicity as shown in Fig. 6b. Only a slight variation can be observed in WBC values for these three groups. However, for the NFH-nBSA group, both WBC and PLT values show mildly apparent difference in comparison with the control group.

To monitor any potential toxic effects of the delivery systems on the treated mice, series of tests for serum biochemistry indexes were carried out. Compared with the serum electrolytes results of control group, the three TAT conjugated groups show barely any differences and much higher than the results of PD mice. The NFH-nBSA group only shows insignificant deviation on the basis of control group (Fig. 6c). For the enzymes and lipids in serum biochemistry studies, we selected important levels of triglyceride (TG), creatine kinase (CK), lactic dehydrogenase (LDH), alanine aminotransferase (ALT) and aspartate aminotransferase (AST). For the three TAT-conjugated nanoparticles, all these five parameters of enzymes and lipids are normal compared with the results of healthy control group except an acceptable decrease in CK results (Fig. 6d). Nevertheless, the results for TG, CK and LDH in NFH-nBSA treated PD mice all show obvious drop as shown in Fig. 6d, indicating that the therapeutic effects of Parkinsonian symptoms is poorer than the TAT-modified groups. The indicators of kidney function, liver and gallbladder function including indirect bilirubin (IBIL), total bilirubin (TB), direct bilirubin (DB), blood urea nitrogen (BUN) and serum creatinine (CRE-E) are also normal for the TAT-conjugated three delivery systems (Fig. 6e). Only the results for CRE-E show an acceptable deviation in these three groups. Specifically, normal blood urea levels represent that kidney and liver function is good. The damage or renal dysfunction may increase urea level in blood. And lower level than normal always indicates liver disease or injury. As shown in Fig. 6e, both BUN and

CRE-E values for TAT-NFH-nBSA nanoparticles are within normal ranges, and are similar to those of control group. The hepatic indicators IBIL, TB, DB and BUN/CRE-E are measured periodically, and show no sign of obvious liver injuries for the drug delivery systems. All these parameters of blood and serum of the TAT-NFH-nBSA nanoparticles are within normal ranges and are similar to values of healthy mice indicating normal kidney, liver and gall bladder function, even after 30 days treatment. Beyond that, in comparison with PD mice, the TAT-NFH-nBSA nanoparticles show excellent therapeutic effects of Parkinsonian symptoms, while the NFH-nBSA group is poor in reversion of the symptoms.

CONCLUSIONS

The abnormal iron accumulation in PD can induce the death of dopaminergic neurons, generation of excessive ROS and finally loss of motor control. Currently, iron chelation therapy has emerged as one effective method for the treatment of PD, which can retard the degeneration of dopaminergic neurons and provide promising neuroprotective strategies. Despite achieving exciting performances in PD treatment recently, the therapeutic efficacy of iron chelators is usually impeded due to their short *in vivo* life time, side effects and saturation in blood circulation before reaching brain lesion sites. Therefore, an ideal iron chelator should possess particular features such as high iron binding affinity, brain-permeability, non-toxicity and the most important factor of delayed saturation capacity, which could be adequately protected from the chelation of free ions in blood circulation.

Using a combination of zwitterionic polymer PMPC as a hydration protective layer and cell penetrating peptide TAT as a BBB-permeable shuttle, we provide adequate evidence

that NFH-loaded iron chelation nanoparticles can be an exceptionally powerful therapeutic option for PD. Most importantly, with suitable protection out of the iron chelators, the drug delivery system can possess delayed saturation feature especially during blood circulation, much longer blood circulation time and much more powerful therapeutic potential for PD mice. This facile synthesis method of the iron chelator loaded therapeutic nanoparticles shows distinct size, structure, circulation behavior and excellent ability in penetrating the BBB. The therapeutic nanoparticles TAT-NFH-nBSA can efficiently accumulate in brain and produce a powerful neuroprotective effect both *in vitro* and *in vivo* for PD treatment. These findings indicate that this novel iron chelator system with a high affinity for Fe ions, long *in vivo* life time and delayed saturation feature can be a valuable tool for PD therapy in the future. Moreover, these iron chelation therapeutic nanoparticles promise an unparalleled approach for delivering other kind of therapeutics to CNS in the treatment of many life-threatening neurodegenerative disorders, including those lacking effective pharmacotherapy.

ASSOCIATED CONTENT

Supporting Information

Supporting movies for non-treated PD mice, NFH-nBSA treated mice and TAT-5-NFH-nBSA treated mice.

AUTHOR INFORMATION

Corresponding Author

*E-mail: X. Z. (xyzhu@sjtu.edu.cn); X. J. (jxcindy@sjtu.edu.cn), Tel.: +86-21-54746215. Fax: +86-21-54741297.

Author contributions

X. Z. planed and supervised the project. N. W., X. J. and X. Z. designed and carried out the detailed experiments, participated in result analysis and wrote the whole paper. N. W. prepared the materials and carried out the spectroscopic measurements, imaging and evaluation *in vitro* and *in vivo*. D. G. assisted with the materials preparation. G. T. assisted with the TEM measurements. All authors critically revised the manuscript.

Notes

The authors declare no competing financial interest.

ACKNOWLEDGMENTS

This work is supported by the National Basic Research Program of China (2015CB931801) National Key Research and Development Plan of China (2016YFA0201500), and National Natural Science Foundation of China (51690151, 51503122). We thank Dr. Yajuan Zou from Instrumental Analysis Center of Shanghai Jiao Tong University for the ICP-AES measurements of series of nanoparticles.

REFERENCES

1. Engelhardt, B. *Science* **2011**, *334*, 1652-1653.

2. Pahuja, R.; Seth, K.; Shukla, A.; Shukla, R. K.; Bhatnagar, P.; Chauhan, L. K. S.; Saxena, P. N.; Arun, J.; Chaudhari, B. P.; Patel, D. K.; Singh, S. P.; Shukla, R.; Khanna, V. K.;

Kumar, P.; Chaturvedi, R. K.; Gupta, K. C. *ACS Nano* **2015**, *9*, 4850-4871.

3. Xie, C. L.; Zhang, Y. Y.; Wang, X. D.; Chen, J.; Chen, Y. H.; Pa, J. L.; Lin, S. Y.; Lin, H. Z.; Wang, W. W. *Neurol. Sci.* **2015**, *36*, 1319-1329.

4. Lang, A. E. *Nat. Med.* **2010**, *16*, 1223-1226.

5. Schnabel, J. *Nature* **2010**, *466*, S2-S5.

6. Schapira, A. H. V; Olanow, C. W.; Greenamyre, J. T.; Bezard, E. *Lancet* **2014**, *384*, 545-55.

7. Haass, C.; Kahle, P. J. *Nature* **2000**, *404*, 341-343.

8. Das, B.; Vedachalam, S.; Luo, D.; Antonio, T.; Reith, M. E. A.; Dutta, A. K. *J. Med. Chem.* **2015**, *58*, 9179−9195.

9. Hunot, S.; Boissiere, F.; Faucheux, B.; Brugg, B.; Mouatt-Prigent, A.; Agid, Y.; Hirsch, E. C. *Neuroscience* **1996**, *72*, 355-363.

10. Chan, C. S.; Guzman, J. N.; Ilijic, E.; Mercer, J. N.; Rick, C.; Tkatch, T.; Meredith, G. E.; Surmeier, D. J. *Nature* **2007**, *447*, 1081-1086.

11. Kalia, L. V.; Lang, A. E. *The Lancet* **2015**, *386*, 896-912.

12. Fahn, S. *Mov. Disord.* **2015**, *30*, 4-18.

13. Fan, C. H.; Ting, C. Y.; Lin, C. Y; Chan, H. L.; Chang, Y. C.; Chen, Y. Y.; Liu, H. L.; Yeh, C. *Sci. Rep.* **2016**, *6*, 19579.

14. Obeso, J. A.; Rodriguez-Oroz, M. C.; Goetz, C. G.; Marin, C.; Kordower, J. H; Rodriguez, M.; Hirsch, E. C; Farrer, M.; Schapira, A. H. V; Halliday, G. *Nat. Med.* **2010**, *16*, 653-661.

15. Ayton, S., Lei, P.; Adlard, P. A; Volitakis, I.; Cherny, R. A; Bush, A. I; Finkelsteinet, D.

I *Mol. Neurodegener.* **2014**, *9*, 1-6.

16. Sofic, E; Riederer, P.; Heinsen, H.; Beckmann, H.; Reynolds, G. P.; Hebenstreit, G.; Youdim, M. B. H. *J. Neural. Transm.* **1988**, *74*, 199-205.

17. Berg, D.; Gerlach, M.; Youdim, M. B. H.; Double, K. L.; Zecca, L.; Riederer, P.; Becker, G. *J. Neurochem.* **2001**, *79*, 225-236.

18. Moos, T.; Morgan, EH. *Ann. N. Y. Acad. Sci.* **2004**, *1012*, 14-26.

19. Ward, R. J.; Zucca, F. A.; Duyn, J. H.; Crichton, R. R.; Zecca, L. *Lancet Neurol.* **2014**, *13*, 1045-1060.

20. Jin, L.; Wang, J.; Zhao, L.; Jin, H.; Fei, G. Q.; Zhang, Y. W.; Zeng, M. S.; Zhong, C. J. *Brain* **2011**, *134*, 50-58.

21. Kaur, D.; Andersen, J. K. *Aging Cell* **2002**, *1*, 17-21.

22. Kaur, D.; Andersen, J. *Ageing Res. Rev.* **2004**, *3*, 327-343.

23. Lee, J. C.; Gray, H. B.; Winkler, J. R. *J. Am. Chem. Soc.* **2008**, *130*, 6898-6899.

24. Langston, J. W.; Schule, B.; Rees, L.; Nichols, R. J.; Barlow, C. *Nat. Genet.* **2015**, *47*, 1378-1384.

25. Goedert, M.; Cheng, Y. *Nature* **2015**, *525*, 458-459.

26. Lei, P.; Ayton, S.; Finkelstein, D. I.; Spoerri, L.; Ciccotosto, G. D.; Wright, D. K.; Wong, B. X. W.; Adlard, P. A.; Cherny, R. A.; Lam, L. Q.; Roberts, B. R.; Volitakis, I.; Egan, G. F.; McLean, C. A.; Cappai, R.; Duce, J. A.; Bush, A. I. *Nat. Med.* **2012**, *18*, 291-295.

27. Zhang, X.; Xie, W.; Qu, S.; Pan, T.; Wang, X.; Le, W. *Biochem. Biophys. Res. Commun.* **2005**, *333*, 544-549.

28. Dexter, D. T.; Statton, S. A.; Whitmore, C.; Freinbichler, W.; Weinberger, P.; Tipton,

K. F.; Corte, L. D.; Ward, R. J.; Crichton, R. R. *J. Neural. Transm.* **2011**, *118*, 223-231.

29. Weinreb, O.; Mandel, S.; Youdim, M. B.; Amit, T. *Free Radic. Biol. Med.* **2013**, *62*, 52-64.

30. Stankowski, J. N.; Dawson, V. L.; Dawson, T. M. *Nat. Med.* **2012**, *18*, 197-198.

31. Ayton, S.; Lei, P.; Duce, J. A.; Wong, B. X. W.; Sedjahtera, A.; Adlard, P. A.; Bush, A. I.; Finkelstein, D. I. *Ann. Neurol.* **2013**, *73*.

32. Lan, J.; Jiang, D. H. *J. Neural. Transm.* **1997**, *104*, 469-481.

33. Rossi, N. A.; Mustafa, I.; Jackson, J. K.; Burt, H. M.; Horte, S. A.; Scott, M. D.; Kizhakkedathu, J. N.; *Biomaterials* **2009**, *30*, 638-648.

34. Imran, M.; Hamilton, J. L.; Lai, B. F. L.; Shenoi, R. A.; Horte, S.; Constantinescu, I.; Leitch, H. A.; Kizhakkedathu, J. N. *ACS Nano* **2013**, *7*, 10704-10716.

35. Goswami, D.; Machini, M. T.; Silvestre, D. M.; Nomura, C. S.; Esposito, B. P. *Bioconjug. Chem.* **2014**, *25*, 2067-2080.

36. Yassin, M. S.; Ekblom, J.; Xilinas, M.; Gottfries, C. G.; Oreland, L. *J. Neurol. Sci.* **2000**, *173*, 40-44.

37. Kaur, D.; Yantiri, F.; Rajagopalan, S.; Kumar, J.; Mo, J. Q.; Boonplueang, R.; Viswanath, V.; Jacobs, R.; Yang, L.; Beal, M. F.; DiMonte, D.; Volitaskis, I.; Ellerby, L.; Cherny, R. A.; Bush, A. I.; Andersen, J. K. *Neuron* **2003**, *37*, 899-909.

38. Levites, Y.; Youdim, M. B. H.; Maor, G.; Mandel, S. *Biochem. Pharmacol.* **2002**, *63*, 21-29.

39. Mandel, S. A.; Avramovich-Tirosh, Y.; Reznichenko, L.; Zheng, H. L.; Weinreb, O.; Amit, T.; Youdim, M. B.H. *Neuro-Signals* **2005**, *14*, 46-60.

40. Youdim, M. B. H.; Stephenson, G.; Shachar, D. B. *Ann. N. Y. Acad. Sci.* **2004**, *1012*, 306-325.

41. Gal, S.; Zheng, H.; Fridkin, M.; Youdim, M. B. *J. Neurochem.* **2005**, *95*, 79-88.

42. Xu, Q.; Kanthasamy, A. G.; Reddy, M. B. *Toxicology* **2008**, *245*, 101-108.

43. Youdim, M. B.; Fridkin, M.; Zheng, H. *Mech. Ageing Dev.* **2005**, *126*, 317-326.

44. Liddell, J. R.; Obando, D.; Liu, J.; Ganio, G.; Volitakis, I.; Moka, S. S.; Crouch, P. J.; White, A. R.; Codd, R. *Free Radic. Biol. Med.* **2013**, *60*, 147-156.

45. Zheng, H.; Youdim, M. B. H.; Fridkin, M. *ACS Chem. Biol.* **2010**, *5*, 603-610.

46. Athauda, D.; Foltynie, T. *Nat. Rev. Neurol.* **2015**, *11*, 25-40.

47. Ali, I. U.; Chen, X. *ACS Nano* **2015**, *9*, 9470-9474.

48. Bai, T.; Sun, F.; Zhang, L.; Sinclair, A.; Liu, S.; Ella-Menye, J. R.; Zheng, Y.; Jiang, S. Y. *Angew. Chem. Int. Ed.* **2014**, *53*, 12729-12734.

49. Cao, Z.; Jiang, S. *Nano Today* **2012**, *7*, 404-413.

50. Zhang, P.; Sun, F.; Tsao, C.; Liu, S. J.; Jain, P.; Sinclair, A.; Hung, H. C.; Bai, T.; Wu, K.; Jiang, S. Y. *Proc. Natl. Acad. Sci.* **2015**, *112*, 12046-12051.

51. Jiang, S.; Cao, Z. *Adv. Mat.* **2010**, *22*, 920-932.

52. Nakaya, T.; Li, Y. J. *Prog. Polym. Sci.* **1999**, *24*, 143-181.

53. Kudaibergenov, S.; Jaeger, W.; Laschewsky, A. *Adv. Polym. Sci.* **2006**, *201*, 157-224.

54. Kitano, H.; Imai, M.; Mori, T.; Gemmei-Ide, M.; Yokoyama, Y.; Ishihara, K. *Langmuir* **2003**, *19*, 10260-10266.

55. Kitano, H.; Kawasaki, A.; Kawasaki, H.; Morokoshi, S. *J. Colloid Interface Sci.* **2005**, *282*, 340-348.

56. Fathalla, M.; Neuberger, A.; Li, S. C.; Schmehl, R.; Diebold, U.; Jayawickramarajah, J. *J. Am. Chem. Soc.* **2010**, *132*, 9966-9967.

57. Liu, Y.; Carver, J. A.; Ho, L. H.; Elias, A. K.; Musgrave, I. F.; Pukala, T. L. *Biochem. Biophys. Res. Commun.* **2014**, *454*, 295-300.

58. Hayden, E. Y.; Kaur, P.; Williams, T. L.; Matsui, H.; Yeh, S. R.; Rousseau, D. L. *Biochemistry* **2015**, *54*, 4599-4610.

59. Howlett, D.; Cutler, P.; Heales, S.; Camilleri, P. *FEBS Letters* **1997**, *417*, 249-251.

60. Kaplan, I. M.; Wadia, J. S.; Dowdy, S. F. *J. Control. Release* **2005**, *102*, 247-253.

61. Wang, H.; Zhang, S. N.; Liao, Z. Y.; Wang, C. Y.; Liu, Y.; Feng, S. Q.; Jiang, X. G.; Chang, J. *Biomaterials* **2010**, *31*, 6589-6596.

62. Copolovici, D. M.; Langel, K.; Eriste, E.; Langel, Ü. *ACS Nano* **2014**, *8*, 1972-1994.

63. Pearce, T. R.; Shroff, K.; Kokkoli, E. *Adv. Mat.* **2012**, *24*, 3803-3822.

64. Barreto, J. A.; O'Malley, W.; Kubeil, M.; Graham, B.; Stephan, H.; Spiccia, L. *Adv. Mat.* **2011**, *23*, H18-H40.

65. Yan, H.; Wang, L.; Wang, J.; Weng, X.; Lei, H.; Wang, X.; Jiang, L.; Zhu, J.; Lu, W.; Wei, X. *ACS Nano* **2011**, *6*, 410-420.

66. Li, J.; Cai, P.; Shalviri, A.; Henderson, J. T.; He, C.; Foltz, W. D.; Prasad, P.; Brodersen, P. M.; Chen, Y.; DaCosta, R. *ACS Nano* **2014**, *8*, 9925-9940.

67. Qiao, R.; Jia, Q.; Hüwel, S.; Xia, R.; Liu, T.; Gao, F.; Galla, H.-J.; Gao, M. *ACS Nano* **2012**, *6*, 3304-3310.

For Table of Contents Use Only:

Iron Chelation Nanoparticles with Delayed Saturation as an Effective Therapy for Parkinson Disease

Nan Wang, Xin Jin*, Dongbo Guo, Gangsheng Tong, Xinyuan Zhu*